Rotating-Magnetic-Field-Assisted Electrodeposition of Copper for Ambulance Medical Equipment

Syamsuir[1] ✉, **Ferry Budhi Susetyo**[1], **Bambang Soegijono**[2], **Sigit Dwi Yudanto**[3], **Basori**[4], **Maman Kartaman Ajiriyanto**[5], **Daniel Edbert**[6], **Evi Ulina Margaretha Situmorang**[7], **Dwi Nanto**[8], **Cahaya Rosyidan**[9]

[1]Department of Mechanical Engineering, Universitas Negeri Jakarta, 13220, Indonesia
[2]PROUDTEK. Lab, Department of Geoscience, Universitas Indonesia, 16424, Indonesia
[3]Research Center for Metallurgy - National Research and Innovation Agency, 15314, Indonesia
[4]Department of Mechanical Engineering, Universitas Nasional, 12520, Indonesia
[5]Research Center for Nuclear Fuel Cycle and Radioactive Waste Technology – National Research and Innovation Agency, 15314, Indonesia
[6]Department of Microbiology, School of Medicine and Health Sciences, Atma Jaya Catholic University of Indonesia, 14440, Indonesia
[7]Department of Physiology and Physics, School of Medicine and Health Sciences, Atma Jaya Catholic University of Indonesia, 14440, Indonesia
[8]Department of Physics Education, UIN Syarif Hidayatullah, 15412, Indonesia
[9]Department of Petroleum Engineering, Universitas Trisakti, 11440, Indonesia

✉ syamsuir@unj.ac.id

Abstract

This study examines the influence of the application of a rotating magnetic field in the electrodeposition of copper (Cu). During the electrodeposition, five constant magnets were rotated (500 and 800 rpm) towards the bottom of the sample. To investigate deposition rate, surface morphology, phase, structure, corrosion resistance, and hardness in deposited Cu using a weighing scale, a scanning electron microscope equipped with energy dispersive spectroscopy (SEM-EDS), X-ray diffraction (XRD), potentiodynamic polarization, and hardness tester respectively. Bacterial activity was also evaluated through this research. Morphological surface observations showed that the increase in the rotational speed of the magnets during the electrodeposition process led to a smooth surface. A perfect Cu phase covers Al alloy with no oxide. The potentiodynamic polarization demonstrated by the increase in the rotating led to a shift to the more positive value of the corrosion potential. Moreover, the corrosion current also decreases with the increase in the rotating speed of the magnets. Less crystallite size promoted forming a higher hardness and inhibition zone of the Cu films.

Keywords: Electrodeposition; Constant magnet; Potentiodynamic; Bacterial activity

1. Introduction

Recently, medical equipment has used aluminium (Al) as the primary material because of its good castability, formability, and mechanical properties [1]. Unfortunately, harmful microbials that reside on medical equipment cause a patient to become severely infected [2], [3]. Nigam et al. tested 82 random ambulances and found approximately 60.97% contaminant in an interior surface prior to cleaning. Following cleaning, there was evidence of bacterial contamination of 35.37% [4]. Furthermore, exposure to 0.9% sodium chloride (NaCl) in medical equipment also reduces surface quality. This condition could be easily avoided by coating the existing Al with a copper film (Cu) for improved antimicrobial and corrosion resistance. Cu has been found to reduce antimicrobial activity and was used in drinking

water, hospital equipment, and public transportation [5]. Zhang et al. found Cu could be used in therapy for antibacterial [6]. Bacteria like *Staphylococcus aureus* could cause skin infections [7]. Moreover, the bacteria could be transmitted from humans to animals and vice versa [8]. Thus, Al enhancement is needed to effectively reduce microbial activity.

Films generated by electrodeposition have better physical and mechanical properties [9]. Moreover electrodeposition produced uniform coating thickness and very high solid content [10]. Wang et al. fabricated the Cu layer through electrodeposition and found a corrosion current of around 1.17 $\mu A/cm^2$ 3.5 % NaCl solution [11]. In comparison to bare Cu, the corrosion current of bare Cu is 60.6 $\mu A/cm^2$ in a 3.5% NaCl solution [12]. This means that Cu as a layer has less corrosion as compared to bulk. Moreover, Al coated with Cu is expected to be less costly compared to those made by bare Cu [13].

Various studies on electrodeposition in a constant magnetic field have been published recently [14]–[16]. The application of a constant static magnetic field at different intensities was employed for these studies. By adding several magnetic field strengths, the transfer of Cu^{2+} ions from the anode to the cathode can be controlled. The transfer motion of Cu^{2+} ions from the anode to the cathode is close to the deposition rate [17].

So far, an alternate magnetic field has become the new approach to study electrodeposited films. By rotating the magnetic field, the electrodeposition process becomes an alternative to generate better properties. Various spinning 1000, 1500, 2000, 2500, and 3000 rpm of constant magnetic field (1800G) were created with different texture coefficients and nickel (Ni) film structures. In addition, a different surface morphology is observed at 1500 rpm [18]. Various research was also conducted by rotating working electrodes upside constant magnet to investigate the surface chirality of Cu films [19]–[21].

In this study, the effect of the rotating magnetic field on the properties of Cu films was examined to get better quality of the Cu films for medical equipment in the ambulance. The corrosion is focused on 0.9 % NaCl because a concentration of 0.9 % could be found in eccrine sweat and saline-infused for humans [22], [23].

2. Methods

2.1. Material Preparation

The material was used in this research Al alloy (1.63 wt.% Fe, 1.49 wt.% Mg, and Al balance) as the cathode, and a Cu plate was used as the anode. Prior electrodeposition process, the cathode was polished and cleaned with acetone. The electrodeposition process was conducted with 2 mA/cm^2 of current density with 1 hour of electrodeposition time in 250ml analytical copper sulfate solution (0.5 M $CuSO_4$ and 20 ml/l H_2SO_4). Five constant magnets (1400 G) were placed in the Teflon disc (south pole near the cathode) and used in the electrodeposition process (clockwise rotation direction). Samples with no magnet rotation and with magnet rotation (500 rpm and 800 rpm) were CuM0, CuM50, and CuM80, respectively. The apparatus of the electrodeposition process is shown in **Figure 1a** and **Figure 1b**.
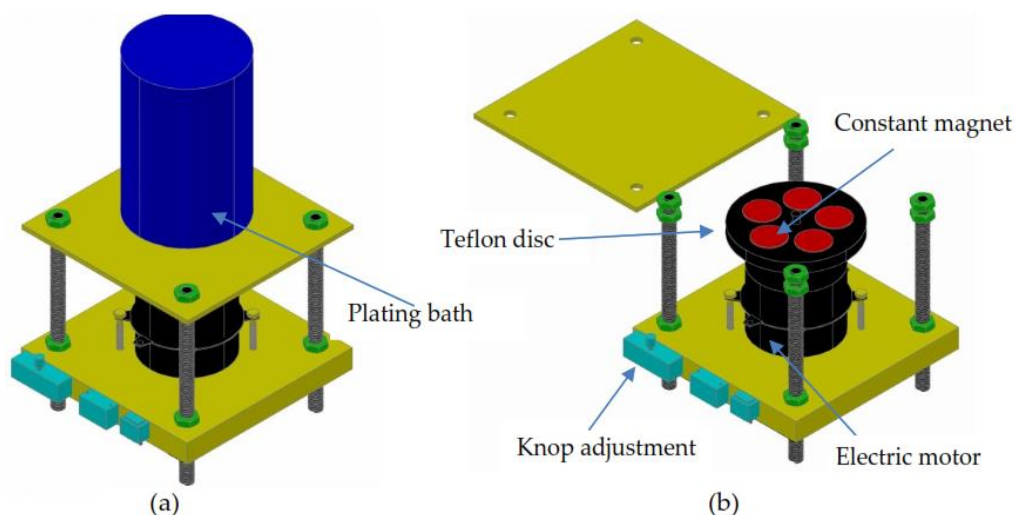

Figure 1. The apparatus of the electrodeposition process: (a) complete apparatus and (b) magnet position

2.2. Deposition Rate

Before and after the electrodeposition process, the samples were weighed with a digital balance. The mass increment for each sample is used in the following expression to calculate the deposition rate [24]:

$$v = \frac{1000\Delta m}{\rho St} \qquad (1)$$

where v is the deposition rate of the Cu sample (μm/h), 1000 is constant, Δm is the mass increment of the Cu sample after deposition (g), ρ is the Cu film density (g/cm³), S is the area of the cathode (cm²), and t is the Cu electrodeposition time (h).

2.3. Scanning Electron Microscope-Energy Dispersive Spectroscopy (SEM-EDS) and Roughness Analysis

SEM FEI Quanta 650, equipped with EDS Oxford Instrument, was used for the observations of the surface morphology of Cu films. A Mathlab technique was used for roughness analysis.

2.4. X-ray Diffraction (XRD)

A PANalytical with Cu Kα1 λ=1.5406 Å and step size 0.02° from 20 – 80° (2θ) was used to observe the crystal structure of the Cu film. The Rietveld method is used to refine diffraction patterns with the assistance of the general structural analysis system (GSAS) computer program [25]. The results obtained from the diffraction pattern analysis were then used as a basis for calculating crystallite size. The Monshi-Scherrer equation was used to estimate crystallite size.

2.5. Potentiodynamic Polarization

The potentiodynamic polarization test solution used 0.9% NaCl obtained from Merk. A Gamry ref 600 potentiostat was used with 0.001 V/s of scan rate to observe Icorr and E_{corr}. Saturated calomel electrode (SCE), platinum (Pt), and Cu sample as reference, counter, and working electrodes, respectively. The corrosion rate would be calculated by adding i$_{corr}$ in the following expression [26]:

$$Cor.Rate = \frac{CMi_{corr}}{n\rho} \qquad (2)$$

where *Cor. Rate* is corrosion rate (mpy), *C* is constant (0.129), *M* is atomic weight (g/mol), i_{corr} is

current density (A/cm²), n is the number of electrons involved, and ρ is density (g/cm³).

2.6. Hardness

Electrodeposited Cu film was measured with an FV-300e Vickers hardness tester. 1 kg of the load was used for indentation, and five spot indentation was collected. The average hardness of the samples was presented in the diagram (**Figure 8**).

2.7. Bacterial Activity Observation

The bacteria used in this investigation is the standard bacteria *Staphylococcus aureus* (ATCC 29213). Antimicrobial effect was evaluated by means of a modified direct contact test. A bacterial suspension with a density of 0.5 McFarland Standard (~ 10^8 CFU/ml) was spread using a cotton swab on Mueller Hinton agar medium. The media was allowed to dry for 1 minute until the suspension seeped into the agar surface. The samples were placed upside down with the test surface facing the agar. The media was incubated at 35 ± 1°C for 24 hours.

3. Results and Discussion

3.1. Deposition Rate

The deposition rate result was calculated from expression (1), as shown in **Figure 2** which shows samples CuM0, CuM50, and CuM80 deposition rates are 50.53, 51.06, and 52.68 μm/h, respectively. Coey and Hinds reported magnetic field influences the deposition rate [27]. The magnet rotating around the electrodeposition sample exerts a magnetic field, which varies perio-
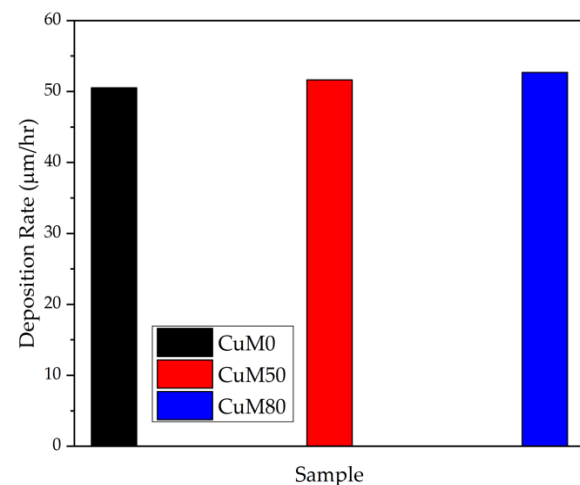
Figure 2. Deposition rates of the sample

dically and induces an Eddy electric field. The Eddy electric field can be attributed to the additional magnetohydrodynamic (MHD) flow convection [18]. The increase in rotational speed led to an increase in deposition rate. Cu^{2+} ions move faster from the anode to the cathode, which is affected by the increased deposition rate. An increased deposition rate would influence a nucleation rate that impacted surface morphology [28], [29]. This phenomenon will be discussed in another section.

3.2. SEM-EDS

The surface morphology and phases of Cu films were examined using SEM-EDS. All samples show faceted structures. Based on Fukunaka et al., a faceted structure could be formed when electrodeposition was performed in 0.05 M $CuSO_4$ using a current density < 10mA/cm^2 [30].

Based on **Figure 3**, the absence of the magnetic field during deposition results in an un-uniform grain of the Cu layer in the Al alloy substrate. On the other hand, by increasing the speed of the magnet, a uniform grain distribution could be achieved. Fahidy found a grain sized Cu becomes fine with a preset magnetic field when electrodeposition was conducted [31]. Matsushima et al. found a magnetic field could influence hydrogen evolution in the cathode surfaces. The superimposition of the magnetic field induces a visible catalytic effect on the evolution of hydrogen and its compact surface [32].

Generally, a higher spinning rate would lead to uniform grain distribution due to the magnetic field delivering the circumference of Cu ions on substrate surfaces [18]. Thus, the rate of nucleation increases with a rise in the spinning magnet. This result is in alignment with the present study.

The EDS observation of the Cu film is seen in **Figure 3**. It can be seen 100% films of Cu without impurities such as oxide (O_2). During the electrodeposition of Cu films, O_2 is also produced as a product of a secondary reaction with the anode. This means that the secondary reaction

does not take place during the production of Cu films [17]. Moreover, O_2 could appear due to sample transport and storage before the EDS examination [33]. Tasic et al. found O_2 on the Cu surface after being immersed 7 days in 0.9% NaCl [34]. Exhibit O_2 would form CuO, which the hardness could influence. Hence, these could be neglected because O_2 invisible in Cu films.

An analytical result of roughness and histogram are seen in **Figure 4**. Roughness evaluation to understand the pixel levels in the grayscale image, the original SEM image is converted to grayscale (from 0 to 255) using MATLAB software, and the corresponding histogram image is obtained [35]. The morphology of the surface roughness of Cu films was analyzed statistically, and the percentage of mass variation (cv) is displayed in the **Table 1** [36]. The higher the cv value, the more roughness the Cu surface. As the rotation increased, the surface was smooth. Additional MHD flow convection by Eddy electric field attributed to arrange movement of the Cu ions to the cathode and confirmed by deposition rate (**Figure 1**). Cu ions are present in greater quantities at higher deposition rates, which could promote a more rapid nucleation rate. This rate allows a physical impact on the growing grain, producing a smooth morphology.

Generally, the roughness of Cu film develops as a result of uneven crystal growth and nucleation. A static magnet could result in uneven crystal growth and nucleation, resulting in rougher surfaces due to an increased concentration gradient at the interface between the electrode and solution [37]. Moreover, hydrogen bubbles at the cathode surfaces act as an obstacle to the magnetic current and influence the inhomogeneous of the current distribution, which could result in rough Cu deposited [38].

3.3. XRD

The diffraction pattern of Cu layers on an Al substrate is shown in **Figure 5**. The peaks of the indexed plane (111), (200), and (220) show that the

Table 1. Roughness properties

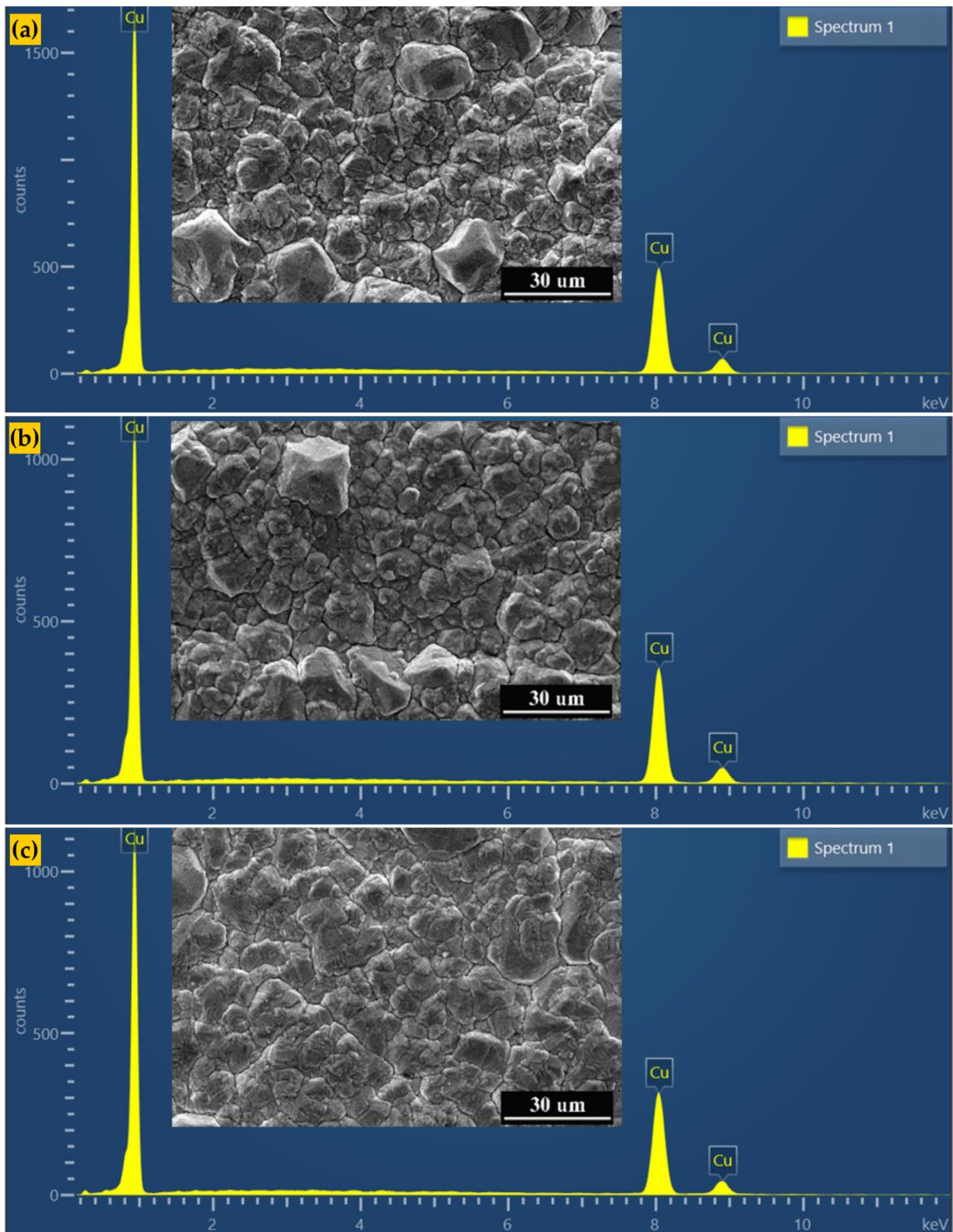| Sample	Average	Standard deviation	cv (%)
CuM0	99.73	46.60	46.73
CuM50	88.09	39.97	45.38
CuM80	99.93	34.58	34.60

Figure 3. SEM-EDS results: (a) CuM0, (b) CuM50, and (c) CuM80

Cu phase is growing on the substrate. According to Roy et al., Qu et al., and Narushima et al. [39]–[41], the peaks of the indexed plane at angles 43.34°, 50.47°, and 74.14° are Cu phase peaks. It can be noticed that the intensity value of the peaks in the Cu phase of the CuM50 sample appears to have the lowest value of the three diffraction patterns [39]–[41]. The variation in this intensity value reflects the variation in the full width at half maximum (FWHM) value and the variation in crystal size. **Table 2** lists the FWHM value for each sample.
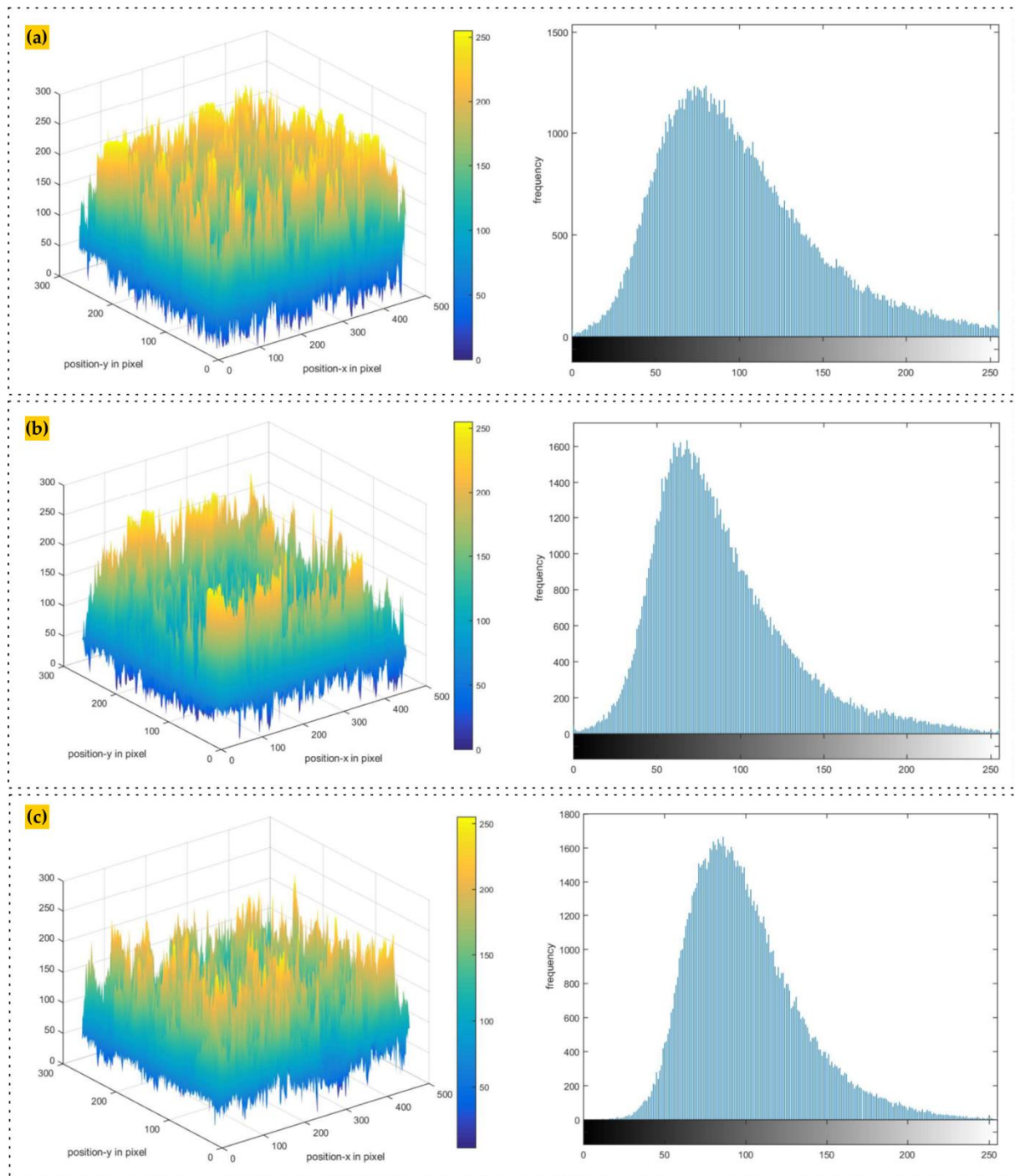
Figure 4. Roughness analysis results and histogram (a) CuM0, (b) CuM50, and (c) CuM80

Figure 6a shows the calculated results for the CuM50 sample with the observed diffraction patterns. The Rietveld method was successfully used to calculate the diffraction patterns. **Table 2** displays the full calculation results for the three samples. According to **Table 2**, all of the samples have the same lattice constant value for the Cu cubic phase (Fm-3m). This suggests that lattice distortion in the Cu phase is not brough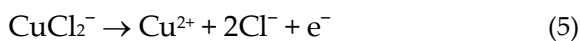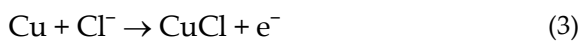t on by the rotating magnetic field. Although no lattice distortion was observed, the rotating magnetic field did cause a change in crystallite size. The Monshi-Scherrer equation was used to estimate the crystallite size of Cu film samples [42]. From the ln (1/cos θ) vs ln FWHM curve for the CuM50 sample shown in **Figure 6b**, we obtain the line equation y=1.6541x-6.4931. The intercept is determined as -6.4931 from the line equation. The intercept value is then inserted into the equation kλ/L=e^intercept [42]. Where k is shape factor (k=0.94),

λ is wavelength of X-ray source (nm), L denotes the crystallite size (nm), θ represents the peak angle (°), and FWHM is the full width at half maximum (radians). The calculated results show that the crystallite size of the CuM50 sample is 95.66 nm. **Table 2** shows an estimation of the crystallite size and lattice constants for various samples.

3.4. *Potentiodinamic Polarization*

The mobile nature of the ambulance activity promoted acceleration of corrosion [43]. The corrosion acceleration could due to eccrine sweat and saline-infused for humans. Therefore potentiodynamic polarization test was carried out in 0.9 % NaCl solution. The potentiodynamic polarization test behaviour can be seen from the **Figure 7**.

The dissolution of the anode of Cu in NaCl can be shown by the following reaction [44], [45]:

$$Cu + Cl^- \rightarrow CuCl + e^- \tag{3}$$

$$CuCl + Cl^- \rightarrow CuCl_2^- \tag{4}$$

$$CuCl_2^- \rightarrow Cu^{2+} + 2Cl^- + e^- \tag{5}$$

CuCl is insoluble and could readily be adsorbed as the first reaction product (eq. 3). The adhesion of the CuCl on the Cu surface is insufficient to protect the corrosion. In the second

reaction, the CuCl transformed into a soluble Cu(I)Cl complex, which could quickly diffuse into a solution [46].

Based on **Figure 7**, increased magnet rotation resulted in a more positive value of potential. This means a higher speed would result in a nobler sample. In some cases, the nobler of the films could reduce a corrosion current [47]. Tasic et al. found a more positive value that reduces the corrosion current when Cu tested in the 0.9% NaCl [34]. The corrosion rate is found and tabulated in **Table 3** by calculating using Eq. (2).
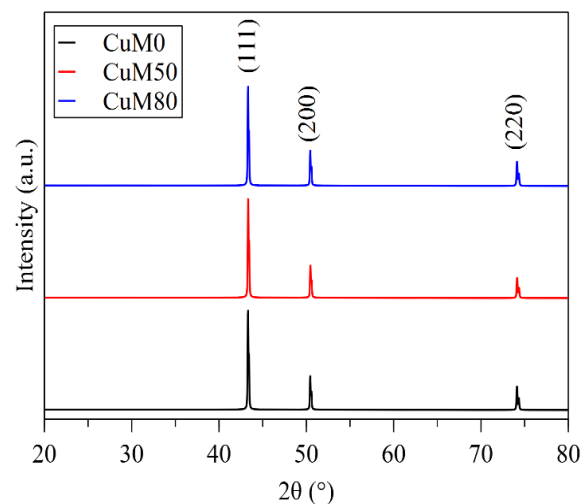

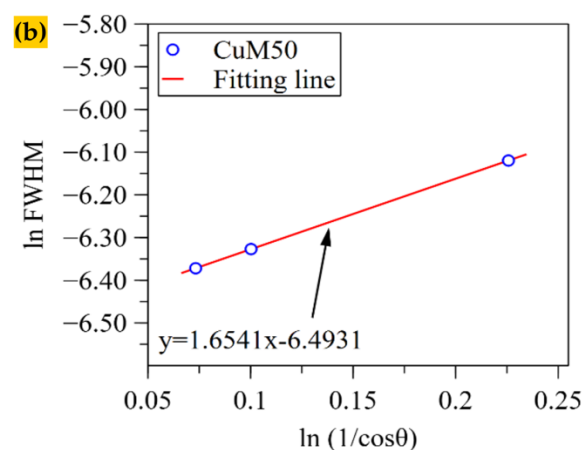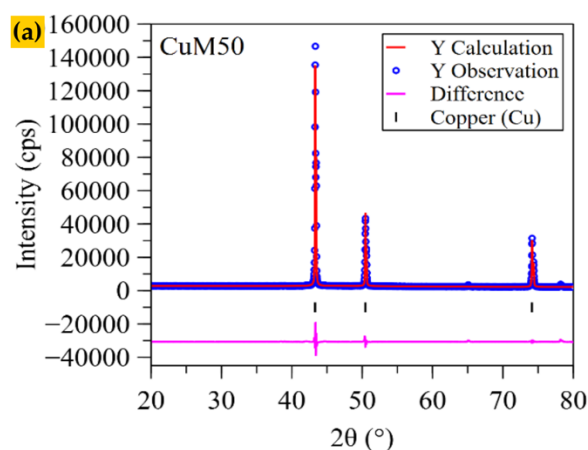
Figure 5. XRD results of CuM0, CuM50, and CuM80 samples

Figure 6. Calculation vs observation of diffraction pattern of the CuM50 sample (a) and Plot of ln (1/cos θ) vs ln FWHM of the CuM50 sample (b)

Table 2. FWHM, lattice constants, and crystallite size

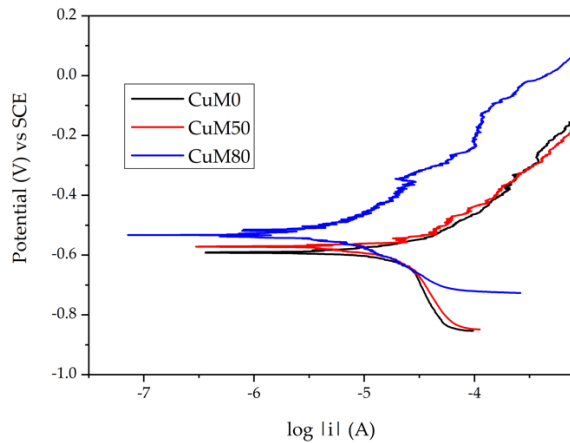| Sample	FWHM (°)			Lattice *a=b=c* (nm)	Crystallite size (nm)
	(111)	(200)	(220)		
CuM0	0.0952	0.0991	0.1194	0.3615	97.16
CuM50	0.0979	0.1024	0.1260	0.3615	95.66
CuM80	0.0943	0.0992	0.1246	0.3615	100.50

Figure 7. Polarization potentiodynamic test results

Based on **Table 3** it can be seen an increase in the speed of the spinning magnet would decrease the corrosion rate. This behaviour may be different from the surface morphology of the samples. The corrosion rate of Cu could decrease by increasing grain size, which perfectly agrees with previous research [15], [48]. Compact morphology also influences to decrease in the corrosion rate [49]. In comparison to the SEM result, a larger grain size and compact morphology are observed in the CUM80 sample. This condition could be confirmed CuM80 sample has better corrosion resistance.

3.5. Hardness

The hardness test was carried out with a weight of 1 kg. The average of the hardness is presented in **Figure 8**. Kumar et al. found bare Cu has a hardness of around 150 HV [50]. Ghosh et al.

reported hardness of the Cu film around 22.94 until 114.7 HV, aligning with this research [51]. Augustin et al. found that a decrease in crystallite size promoted an increased hardness of Cu films on Al substrates [13]. Compared with the **Table 2**, linearly correlation between hardness and crystallite size. Therefore, it can be concluded that the decrease in hardness of the Cu film is caused by the increase in crystallite size.

3.6. Bacterial Activity Observation

Bacterial activity was carried out in 4 samples. The blank sample is a non-coated sample used in the observation for comparison. The bacterial activity observation can be seen in **Figure 9**.

Based on **Table 4**, coated samples have a higher inhibition zone than uncoated. The purity of the deposited Cu has contributed to increase antibacterial activity [13]. The sample CuM50 has
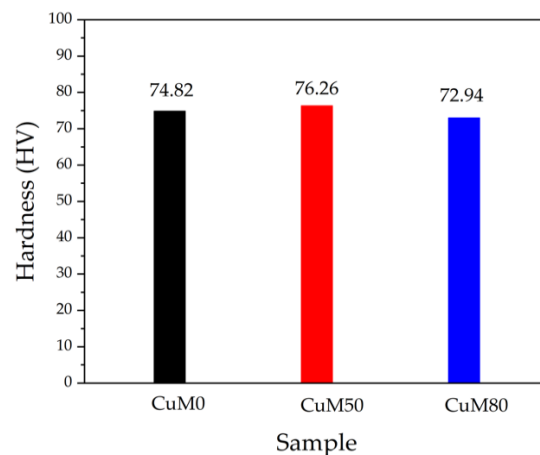
Figure 8. Hardness test results

Table 3. Potentiodynamic polarization result

Sample	E_{corr} (V) vs SCE	i_{corr} (A/cm²)	Cor. Rate (mpy)
CuM0	-0.608	2.48×10^{-5}	22.39
CuM50	-0.592	2.30×10^{-5}	20.81
CuM80	-0.533	7.75×10^{-6}	9.73

Figure 9. Bacterial activity investigation result: (a) Blank, (b) CuM0, (c) CuM50, and (d) CuM80

Table 4. Bacterial activity measurement result
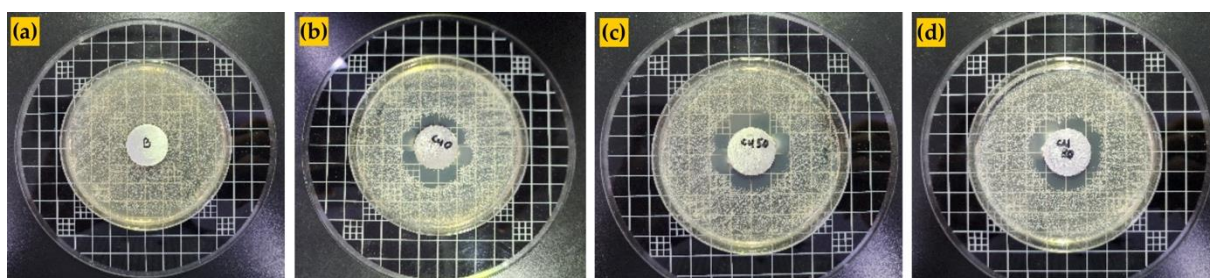
Sample	*Staphylococcus aureus* (ATCC 29213)	
	Inhibition Zone (mm)	Diffusion Distance (mm)
Blank	23	0
CuM0	37±3.5	6.3±3.5
CuM50	40±1	7.6±3.2
CuM80	34±2	6±2.6

a higher inhibition zone than others, probably due to smaller crystallite size. Azzam et al. have found that larger crystallite size could reduce the inhibition zone [52]. Ramyadevi et al. have found an inhibition zone of *Staphylococcus aureus* on Cu nanoparticles around 22 mm [53]. Ahamed et al. have found an inhibition zone of Staphylococcus aureus on Cu nanoparticle (23 nm) around 24 mm [54]. In relation to this research, the inhibition zone is higher than the other studies mentioned above.

Hajduga et al. found that bacterial colonization on the surface is independent of surface roughness when investigating material for modern ambulance's interior [2]. That results perfect agreement with present research where bacterial colonization is independent to surface rougness (See **Table 1** and **Table 4**).

Rago et al. investigated 71 ambulances from 34 different Chicago-area municipalities and found 69% *Staphylococcus aureus* in all ambulances. 77% showed resistance to at least one antibiotic and 34% resistance to two or more antibiotics [55]. Thus, the condition could be solved by Cu coating. As mentioned above, Cu could enhance the inhibition zone of *Staphylococcus aureus*.

4. Conclusion

Electrodeposition Cu influenced by the rotating of magnets was successfully conducted. Surface morphology observations showed that increasing the rotating rate of magnets during the electrodeposition process led to an increase in the deposition rate and formed a smooth surface. In this study, a perfect phase of Cu is exhibited without oxide on the surfaces. Structure observation shows the preferred orientation of the (111) plane on three samples. The potentiodynamic polarization demonstrated by the increase in the rotating led to a shift to the more positive value of the corrosion potential. Moreover, the corrosion rate also decreases with the increase in the rotating rate of the magnets.

Less crystallite size promoted forming a higher hardness and inhibition zone of the Cu films.

_____

Author's Declaration

Authors' contributions and responsibilities

The authors made substantial contributions to the conception and design of the study. The authors took responsibility for data analysis, interpretation and discussion of results. The authors read and approved the final manuscript

Availability of data and materials

All data are available from the authors.

Competing interests

The authors declare no competing interest.

Additional information

No additional information from the authors.
_____

References

[1] Saifudin, N. Muhayat, E. Surojo, Y. H. P. Manurung, and Triyono, "Mitigation of Porosity and Residual Stress on Car Body Aluminum Alloy Vibration Welding: A Systematic Literature Review," *Automotive Experiences*, vol. 5, no. 3, pp. 477–493, 2022, doi: 10.31603/ae.7965.

[2] M. A. Hajduga, S. Węgrzynkiewicz, J. Waś-Solipiwo, M. Hajduga, and M. B. Hajduga, "Innovative solutions from the field of the material science and medicine in the interior of modern ambulances," *Materials Science Forum*, vol. 844, pp. 50–54, 2016, doi:

10.4028/www.scientific.net/MSF.844.50.

[3] R. Rusdjijati, S. A. Subrata, Z. B. Pambuko, M. Setiyo, and M. Noga, "Strategy for Safe Passenger Transport during the COVID-19 Pandemic: From Review to Recommendation," *Automotive Experiences*, vol. 5, no. 2, pp. 90–102, 2022, doi: 10.31603/ae.6593.

[4] Y. Nigam and J. Cutter, "A preliminary investigation into bacterial contamination of Welsh emergency ambulances," *Emergency Medicine Journal*, vol. 20, no. 5, pp. 479–482, 2003, doi: 10.1136/emj.20.5.479.

[5] M. Vincent, P. Hartemann, and M. Engels-Deutsch, "Antimicrobial applications of copper," *International Journal of Hygiene and Environmental Health*, vol. 219, no. 7, pp. 585–591, 2016, doi: 10.1016/j.ijheh.2016.06.003.

[6] N. Zhang, Y. Zheng, Z. Wang, and X. Liu, "Copper(II) based low molecular weight collagen fragments-chlorin e6 nanoparticles synergize anti-cancer and anti-bacteria photodynamic therapy," *Journal of Photochemistry and Photobiology B: Biology*, vol. 232, no. May, 2022, doi: 10.1016/j.jphotobiol.2022.112473.

[7] R. H. Deurenberg and E. E. Stobberingh, "The evolution of Staphylococcus aureus," *Infection, Genetics and Evolution*, vol. 8, no. 6, pp. 747–763, 2008, doi: 10.1016/j.meegid.2008.07.007.

[8] V. Peton and Y. Le Loir, "Staphylococcus aureus in veterinary medicine," *Infection, Genetics and Evolution*, vol. 21, pp. 602–615, 2014, doi: 10.1016/j.meegid.2013.08.011.

[9] Y. Zhang, B. Yuan, L. Li, and C. Wang, "Edge electrodeposition effect of cobalt under an external magnetic field," *Journal of Electroanalytical Chemistry*, vol. 865, p. 114143, 2020, doi: 10.1016/j.jelechem.2020.114143.

[10] S. N. S. Z. Abidin, W. H. Azmi, A. I. Ramadhan, and N. N. M. Zawawi, "Comprehensive Review of Nanoparticles Dispersion Technology for Automotive Surfaces," *Automotive Experiences*, vol. 5, no. 3, pp. 304–327, 2022, doi: 10.31603/ae.6882.

[11] S. H. Wang, X. W. Guo, C. Sun, J. Gong, L. M. Peng, and W. J. Ding, "Electrodeposition of Cu coating with high corrosion resistance on Mg-3.0Nd-0.2Zn-0.4Zr magnesium alloy," *Transactions of Nonferrous Metals Society of China (English Edition)*, vol. 24, no. 12, pp. 3810–3817, 2014, doi: 10.1016/S1003-6326(14)63537-8.

[12] F. M. Al Kharafi, I. M. Ghayad, and R. M. Adallah, "Sulfide induced intergranular corrosion of copper in salt water containing benzotriazole," *e-Journal of Surface Science and Nanotechnology*, vol. 9, no. August, pp. 306–310, 2011, doi: 10.1380/ejssnt.2011.306.

[13] A. Augustin, P. Huilgol, K. R. Udupa, and U. B. K, "Effect of current density during electrodeposition on microstructure and hardness of textured Cu coating in the application of antimicrobial Al touch surface," *Journal of the Mechanical Behavior of Biomedical Materials*, vol. 63, pp. 352–360, 2016, doi: 10.1016/j.jmbbm.2016.07.013.

[14] M. Zieliński, "Effects of constant magnetic field on the electrodeposition reactions and cobalt-tungsten alloy structure," *Materials Chemistry and Physics*, vol. 141, no. 1, pp. 370–377, 2013, doi: 10.1016/j.matchemphys.2013.05.025.

[15] F. B. Susetyo, B. Soegijono, and Yusmaniar, "Effect of a constant magnet position and intensity on a copper layer obtained by DC electrodeposition," *International Journal of Corrosion and Scale Inhibition*, vol. 10, no. 2, pp. 766–782, 2021, doi: 10.17675/2305-6894-2021-10-2-18.

[16] K. Kołodziejczyk *et al.*, "Influence of constant magnetic field on electrodeposition of metals, alloys, conductive polymers, and organic reactions," *Journal of Solid State Electrochemistry*, vol. 22, no. 6, pp. 1629–1674, 2018, doi: 10.1007/s10008-017-3875-x.

[17] B. Soegijono, F. B. Susetyo, Yusmaniar, and M. C. Fajrah, "Electrodeposition of paramagnetic copper film under magnetic field on paramagnetic aluminum alloy substrates," *e-Journal of Surface Science and Nanotechnology*, vol. 18, pp. 281–288, 2020, doi: 10.1380/EJSSNT.2020.281.

[18] T. Wang and W. Chen, "Effects of Rotating Magnetic Fields on Nickel Electro-Deposition," *ECS Electrochemistry Letters*, vol. 4, no. 6, pp. D14–D17, 2015, doi: 10.1149/2.0101506eel.

[19] I. Mogi, R. Morimoto, R. Aogaki, and K. Takahashi, "Surface chirality in rotational magnetoelectrodeposition of copper films,"

Magnetochemistry, vol. 5, no. 3, pp. 2–9, 2019, doi: 10.3390/magnetochemistry5030053.

[20] I. Mogi, R. Morimoto, R. Aogaki, and K. Watanabe, "Surface chirality induced by rotational electrodeposition in magnetic fields," 2013. doi: 10.1038/srep02574.

[21] R. Morimoto *et al.*, "Theory of Chiral Electrodeposition by Chiral Micro- and Nano-Vortices under a Vertical Magnetic Field -1: 2D Nucleation by Micro-Vortices," *Magnetochemistry*, vol. 8, no. 7, pp. 1–66, 2022, doi: 10.3390/magnetochemistry8070071.

[22] J. W. Bond and E. Lieu, "Electrochemical behaviour of brass in chloride solution concentrations found in eccrine fingerprint sweat," *Applied Surface Science*, vol. 313, pp. 455–461, 2014, doi: 10.1016/j.apsusc.2014.06.005.

[23] K. Bin Tayyab, A. Farooq, A. A. Alvi, A. B. Nadeem, and K. M. Deen, "Corrosion behavior of cold-rolled and post heat-treated 316L stainless steel in 0.9wt% NaCl solution," *International Journal of Minerals, Metallurgy and Materials*, vol. 28, no. 3, pp. 440–449, 2021, doi: 10.1007/s12613-020-2054-8.

[24] J. Lu, M. Wang, X. Deng, J. Yan, J. Yun, and S. Jiao, "Evaluation of K3Fe(CN)6 on Deposition Behavior and Structure of Electroless Copper Plating," *Electrochemistry*, vol. 87, no. 4, pp. 214–219, 2019.

[25] A. C. Larson and R. B. Von Dreele, *General Structure Analysis System (GSAS)*, vol. 748. Los Alamos: University of California, 2004.

[26] Z. Ahmad and Zaki Ahmad, *Principles of Corrosion Engineering and Corrosion Control*, 1st ed., no. September. Oxford, United Kingdom: Butterworth-Heinemann, 2006.

[27] J. M. D. Coey and G. Hinds, "Magnetic electrodeposition," *Journal of Alloys and Compounds*, vol. 326, pp. 238–245, 2001.

[28] A. Augustin, K. Rajendra Udupa, and K. Udaya Bhat, "Effect of coating current density on the wettability of electrodeposited copper thin film on aluminum substrate," *Perspectives in Science*, vol. 8, pp. 472–474, 2016, doi: 10.1016/j.pisc.2016.06.003.

[29] R. Sekar, "Synergistic effect of additives on electrodeposition of copper from cyanide-free electrolytes and its structural and morphological characteristics," *Transactions of Nonferrous Metals Society of China (English Edition)*, vol. 27, no. 7, pp. 1665–1676, 2017, doi: 10.1016/S1003-6326(17)60189-4.

[30] Y. Fukunaka, H. Doi, and Y. Kondo, "Structural Variation of Electrodeposited Copper Film with the Addition of an Excess Amount of H2SO4," *Journal of The Electrochemical Society*, vol. 137, no. 1, pp. 88–93, 1990, doi: 10.1149/1.2086445.

[31] T. Z. Fahidy, "Characteristics of surfaces produced via magnetoelectrolytic deposition," *Progress in Surface Science*, vol. 68, no. 4–6, pp. 155–188, 2001, doi: 10.1016/S0079-6816(01)00006-5.

[32] H. Matsushima, A. Bund, W. Plieth, S. Kikuchi, and Y. Fukunaka, "Copper electrodeposition in a magnetic field," *Electrochimica Acta*, vol. 53, no. 1, pp. 161–166, 2007, doi: 10.1016/j.electacta.2007.01.043.

[33] F. B. Susetyo, M. C. Fajrah, and B. Soegijono, "Effect of Electrolyte Temperature on Properties of Nickel Film Coated onto Copper Alloy Fabricated by Electroplating," *e-Journal of Surface Science and Nanotechnology*, vol. 18, pp. 223–230, 2020, doi: 10.1380/ejssnt.2020.223.

[34] Ž. Z. Tasić, M. B. Petrović Mihajlović, M. B. Radovanović, A. T. Simonović, and M. M. Antonijević, "Cephradine as corrosion inhibitor for copper in 0.9% NaCl solution," *Journal of Molecular Structure*, vol. 1159, pp. 46–54, 2018, doi: 10.1016/j.molstruc.2018.01.031.

[35] A. Srivani and M. Anthony Xavior, "Investigation of surface texture using image processing techniques," *Procedia Engineering*, vol. 97, pp. 1943–1947, 2014, doi: 10.1016/j.proeng.2014.12.348.

[36] S. Rwawiire, "Prediction of polyester/cotton ring spun yarn unevenness using adaptive neuro fuzzy inference system," *Journal of Textile and Apparel, Technology and Management*, vol. 8, no. 4, 2014.

[37] A. Fattahi and M. E. Bahrololoom, "Investigating the effect of magnetic field on pulse electrodeposition of magnetic and non-magnetic nanostructured metals," *Surface and Coatings Technology*, vol. 261, pp. 426–435, 2015, doi: 10.1016/j.surfcoat.2014.10.013.

[38] J. A. Koza *et al.*, "Hydrogen evolution under the influence of a magnetic field," *Electrochimica Acta*, vol. 56, no. 6, pp. 2665–

2675, 2011, doi: 10.1016/j.electacta.2010.12.031.

[39] K. Roy, C. K. Sarkar, and C. K. Ghosh, "Antibacterial mechanism of biogenic copper nanoparticles synthesized using Heliconia psittacorum leaf extract," *Nanotechnology Reviews*, vol. 5, no. 6, pp. 529–536, 2016, doi: 10.1515/ntrev-2016-0040.

[40] D. Qu *et al.*, "Preparation of graphene nanosheets/copper composite by spark plasma sintering," *Advanced Materials Research*, vol. 833, no. December 2015, pp. 276–279, 2014, doi: 10.4028/www.scientific.net/AMR.833.276.

[41] T. Narushima, H. Tsukamoto, and T. Yonezawa, "High temperature oxidation event of gelatin nanoskin-coated copper fine particles observed by in situ TEM," *AIP Advances*, vol. 2, no. 4, 2012, doi: 10.1063/1.4759498.

[42] A. Monshi, M. R. Foroughi, and M. R. Monshi, "Modified Scherrer Equation to Estimate More Accurately Nano-Crystallite Size Using XRD," *World Journal of Nano Science and Engineering*, vol. 02, no. 03, pp. 154–160, 2012, doi: 10.4236/wjnse.2012.23020.

[43] A. Bielawska-Drózd *et al.*, "Identification and characteristics of biological agents in work environment of medical emergency services in selected ambulances," *International journal of occupational medicine and environmental health*, vol. 30, no. 4, pp. 617–627, 2017, doi: 10.13075/ijomeh.1896.00816.

[44] W. Li, L. Hu, S. Zhang, and B. Hou, "Effects of two fungicides on the corrosion resistance of copper in 3.5% NaCl solution under various conditions," *Corrosion Science*, vol. 53, no. 2, pp. 735–745, 2011, doi: 10.1016/j.corsci.2010.11.006.

[45] Sudheer and M. A. Quraishi, "Electrochemical and theoretical investigation of triazole derivatives on corrosion inhibition behavior of copper in hydrochloric acid medium," *Corrosion Science*, vol. 70, pp. 161–169, 2013, doi: 10.1016/j.corsci.2013.01.025.

[46] D. Wang, B. Xiang, Y. Liang, S. Song, and C. Liu, "Corrosion control of copper in 3.5 wt.% NaCl Solution by Domperidone: Experimental and Theoretical Study," *Corrosion Science*, vol. 85, pp. 77–86, 2014, doi:

10.1016/j.corsci.2014.04.002.

[47] O. A. Abdullatef, "Chemical and Electrochemical studies on the corrosion of mild-steel, copper and zinc in 0. 5 M H2SO4 solution in presence of Azithromycin as effective corrosion inhibitor," *Journal of Advances in Chemistry*, vol. 10, no. 1, pp. 2146–2161, 2014.

[48] H. Yang, Y. Chen, H. Feng, P. Yang, J. Zhang, and B. Shu, "Optimized corrosion resistance in pure copper via surface mechanical attrition treatment and subsequent annealing," *Materials Today Communications*, vol. 35, no. January, p. 105645, 2023, doi: 10.1016/j.mtcomm.2023.105645.

[49] E. Pellicer *et al.*, "A comparison between fine-grained and nanocrystalline electrodeposited Cu-Ni films. Insights on mechanical and corrosion performance," *Surface and Coatings Technology*, vol. 205, no. 23–24, pp. 5285–5293, 2011, doi: 10.1016/j.surfcoat.2011.05.047.

[50] M. Kumar, G. Ji, and R. Prakash, "Materials Today : Proceedings Investigation on the effects of cooling rate on surface Texture , corrosion behaviour and hardness of pure copper," in *Materials Today: Proceedings*, 2021, vol. 47, no. 19, pp. 6693–6695, doi: 10.1016/j.matpr.2021.05.115.

[51] S. Ghosh, "Electroless copper deposition: A critical review," *Thin Solid Films*, vol. 669, no. November 2018, pp. 641–658, 2019, doi: 10.1016/j.tsf.2018.11.016.

[52] A. Azam, A. S. Ahmed, M. Oves, M. S. Khan, and A. Memic, "Size-dependent antimicrobial properties of CuO nanoparticles against Gram-positive and -negative bacterial strains," *International Journal of Nanomedicine*, vol. 7, pp. 3527–3535, 2012, doi: 10.2147/IJN.S29020.

[53] J. Ramyadevi, K. Jeyasubramanian, A. Marikani, G. Rajakumar, and A. A. Rahuman, "Synthesis and antimicrobial activity of copper nanoparticles," *Materials Letters*, vol. 71, pp. 114–116, 2012, doi: 10.1016/j.matlet.2011.12.055.

[54] M. Ahamed, H. A. Alhadlaq, M. A. M. Khan, P. Karuppiah, and N. A. Al-Dhabi, "Synthesis, characterization, and antimicrobial activity of copper oxide nanoparticles," *Journal of Nanomaterials*, vol. 2014, no. Mic, 2014, doi: 10.1155/2014/637858.

[55] J. V. Rago, L. K. Buhs, V. Makarovaite, E. Patel, M. Pomeroy, and C. Yasmine, "Detection and analysis of Staphylococcus aureus isolates found in ambulances in the Chicago metropolitan area," *American Journal of Infection Control*, vol. 40, no. 3, pp. 201–205, 2012, doi: 10.1016/j.ajic.2011.08.021.